

1 **The changing character of twenty-first century precipitation over the**
2 **western United States in the variable-resolution CESM**

3 Xingying Huang, * Paul A. Ullrich

4 *Department of Land, Air and Water Resources, University of California, Davis*

5 *Corresponding author address: Xingying Huang, Department of Land, Air and Water Resources,
6 University of California Davis, Davis, CA 95616.
7 E-mail: xyhuang@ucdavis.edu

ABSTRACT

8 (To be added once the main content settled down)

9 **1. Introduction**

10 There is substantial and growing interest in understanding the character of precipitation within
11 a changing climate, in large part because of the pronounced impacts of water availability on
12 socioeconomic and natural systems (Hegerl et al. 2004; Kharin et al. 2007; Scoccimarro et al.
13 2013). Among these studies, precipitation extremes have been a major focus, particularly drought
14 and flood events (Seneviratne et al. 2012). Studies examining the character of precipitation in a
15 warming world, which utilize models of varying complexity from simple thermodynamic models
16 through complex coupled climate simulations, suggest that although atmospheric water vapor is
17 increasing, the consequences for precipitation are far more complicated. Extreme precipitation
18 events are particularly nuanced: Our best projections suggest that extreme precipitation events
19 will intensify even in regions where mean precipitation decreases (Tebaldi et al. 2006; Kharin
20 et al. 2007).

21 Although future climate projections are subject to large uncertainties, climate models are
22 nonetheless one of the most versatile tools for studying climate variability and extremes events
23 in the future (Easterling et al. 2000). Global climate models (GCMs) have often been used to
24 investigate changes in the mean, variability and extremes of climate, as forced with predicted
25 greenhouse gas (GHGs) concentrations and aerosol emissions (Meehl et al. 2006). Several past
26 studies have investigated global impacts (Seneviratne et al. 2012), but studies addressing impacts
27 at local and regional scales are less common. Although increased GHG concentrations have con-
28 tributed to the observed intensification of heavy precipitation events over the tropical ocean (Allan
29 and Soden 2008) and the majority of Northern Hemisphere overland areas Min et al. (2011), these
30 impacts are much more poorly understood at regional scales due to variability at finer spatial scales
31 associated with the atmospheric circulation (Trenberth 2011). As a consequence of this variability,

³² a confident assessment of changes in regional extremes requires both high spatial resolution and a
³³ long integration period.

³⁴ Insufficient regional-scale climate information has been a major outstanding problem in climate
³⁵ science, as stakeholders and water managers typically require fine-scale information on climate
³⁶ impacts in order to effectively develop adaptation and mitigation strategies. In order to reach the
³⁷ scales needed for effective local planning, dynamical downscaling with regional climate models
³⁸ (RCMs) has been typically used to ascertain the frequency, intensity, and duration of extreme
³⁹ events. By only simulating a limited regional domain, RCMs better capture fine-scale dynami-
⁴⁰ cal features under high horizontal resolution (Bell et al. 2004; Frei et al. 2006; Rauscher et al.
⁴¹ 2010; Wehner 2013). Higher resolution can also enable more accurate simulation of precipitation
⁴² extremes, which can be driven by land use, land/water contrast, snow cover, cloudiness and circu-
⁴³ lation patterns associated with topography (Leung et al. 2003a; Diffenbaugh et al. 2005; Salathé Jr
⁴⁴ et al. 2008; Wehner et al. 2010). Diffenbaugh et al. (2005) studied both heat events and wet events
⁴⁵ over the contiguous United States based on RCMs simulation at 25 km horizontal resolution, and
⁴⁶ demonstrated that fine-scale processes were critical for accurate assessment of local- and regional-
⁴⁷ scale climate change vulnerability. Leung et al. (2003b) showed that the higher-resolution RCMs
⁴⁸ yield more realistic precipitation patterns and produce more frequent heavy precipitation over the
⁴⁹ western U.S. (WUS), consistent with observations.

⁵⁰ Despite their success, RCMs also have known issues associated with inconsistency between the
⁵¹ lateral forcing data and the driven RCM, and the menu of physical parameterizations and param-
⁵² eters typically available to RCMs can lead to over-tuning of the model for a particular geographic
⁵³ region or climatological field (McDonald 2003; Laprise et al. 2008; Mesinger and Veljovic 2013).
⁵⁴ Consequently, there has been growing interest in variable-resolution enabled GCMs (VRGCMs)
⁵⁵ to improve regional climate simulations. Unlike RCMs, which require GCM data to drive the sim-

ulation at lateral boundaries, VRGCMs use a unified model with coarse global resolution and enhanced resolution over a specific study region (Staniforth and Mitchell 1978; Fox-Rabinovitz et al. 1997). VRGCMs have demonstrated comparable utility for regional climate studies at a reduced computational cost, particular when compared to uniform-resolution GCMs (Fox-Rabinovitz et al. 2006; Rauscher et al. 2013).

In this paper, we utilize the recently developed variable-resolution option in the Community Earth System Model (VR-CESM). VR-CESM is based on the CESM (and its predecessor, the Community Climate System Model (CCSM)), a family of models that have been used for decades to study the global climate (Neale et al. 2010a; Hurrell et al. 2013). The overall performance of VR-CESM for modeling regional climate in the California and Nevada is detailed in Huang et al. (2016), where it was argued that VR-CESM has competitive biases in comparison to the Weather Research and Forecasting (WRF) model (a traditional RCM) and the uniform-resolution CESM, when evaluating both against high-quality observations and reanalysis. VR-CESM has been used in a number of studies to capture fine-scale atmospheric processes (Zarzycki et al. 2014, 2015; Rhoades et al. 2015). It was also shown that VR-CESM did not suffer from apparent artifacts within the coarse-fine transition region.

This study focuses on changes in the character of precipitation over the 21st Century within the WUS, as predicted from long-term ensemble runs conducted with VR-CESM with a local grid resolution of $\sim 0.25^\circ$. The WUS is known to be particularly vulnerable to hydrological extreme events, particularly floods and droughts (Leung et al. 2003b; Caldwell 2010), and hosts a variety of local features and microclimates associated with its rough and varied topography. Simulations of the future climate are performed in accordance with the representative concentration pathway (RCP) 8.5 scenario, which describes a “business-as-usual” projection for GHGs (Riahi et al. 2011). RCP8.5 is a baseline scenario with updated base year calibration (to 2005) and no

80 explicit climate policy. In this study we focus on a single RCP since end-of-century projections
81 with the substantially more optimistic RCP2.6 scenario have been found to be qualitatively sim-
82 ilar to mid-century RCP8.5 results (which are assessed in this study). Simulations are further
83 conducted in accordance with the Atmospheric Model Intercomparison Project (AMIP) protocol
84 (Gates 1992), a widely-used approach for climate model diagnosis, validation and intercompari-
85 son that imposes global sea surface temperatures (SSTs) and sea ice. By constraining atmospheric
86 boundary conditions at the sea surface, we avoid model biases that are known to exist in the fully
87 coupled configuration (Grodsky et al. 2012; Small et al. 2014) and accept potential uncertainties
88 associated with our choice of SSTs.

89 Changes in the character of precipitation, in terms of frequency and intensity, have been assessed
90 in our study from recent history through the end of 21st century. A comprehensive set of metrics
91 for precipitation extremes have been evaluated from ensemble simulations over the 26-year peri-
92 ods corresponding to historical (1980-2005), mid-century (2025-2050) and end-of-century (2075-
93 2100). We hypothesize that spatial inhomogeneity in local geography and temperature will also
94 result in similarly inhomogeneous impacts on the precipitation field. We expect that teleconnec-
95 tions (specifically the El Niño-Southern Oscillation, ENSO) will have a pronounced impact on
96 precipitation features over particular area under the changes of mean SST and its variations. Since
97 only one SST dataset was used for this study, we note that our projections are conditioned on a
98 particular future character of ENSO. This is a potentially large source of uncertainty, as at present
99 there is no clear consensus on how ENSO may behave under a warming climate (Fedorov and
100 Philander 2000; Guilyardi et al. 2009), and strengthening or weakening of this pattern will have
101 clear consequences for our results.

102 This work builds on a number of previous studies that have explored the projected future change
103 in WUS precipitation. For example, Kim (2005) applied downscaled climate change signals to se-

104 lected indicators, and concluded that global warming induced by increased CO₂ is likely to drive
105 increases in extreme hydrologic events in the WUS. Duffy et al. (2006) found that mean precip-
106 itation predicted by the RCMs are not statistically significant compared to interannual variability
107 in many regions over WUS, although there is little consistency among the different RCMs as to
108 responses in precipitation to increased GHGs. Gao et al. (2015) pointed out a potentially large
109 increase in atmospheric river events by the end of the 21st century under the RCP8.5 scenario.

110 This paper is structured as follows. Section 2 describes the model setup. Section 3 describes
111 the methodology and reference datasets employed. An assessment of the ability of the model to
112 capture the climatology of the WUS is given in section 4. Results from the future mean climato-
113 logical trend and projected changes to precipitation indices are in section 6. Section 7 summarizes
114 the main points of the study along with further discussion.

115 2. Model Setup

116 CESM is a state-of-the-art Earth modeling framework, consisting of coupled atmosphere, ocean,
117 land and sea ice models (Neale et al. 2010b; Hurrell et al. 2013). In this study, the Community At-
118 mosphere Model version 5 (CAM5) (Neale et al. 2010b) and the Community Land Model version
119 4.0 (Oleson et al. 2010) are used. CAM5 is configured with the Spectral Element (SE) dynamical
120 core, which supports desirable conservation, accuracy and parallel scalability properties (Dennis
121 et al. 2011; Taylor 2011) and incorporates the variable-resolution option (Zarzycki et al. 2014).
122 CLM is employed in the *unigrid* configuration, which allows the land model and atmospheric
123 model to utilize the same model grid so eliminates the need for interpolation. SSTs and sea ice,
124 which are used to compute ocean-atmosphere fluxes, are prescribed in accordance with the AMIP
125 protocol (Gates 1992). The variable-resolution mesh used for this study is depicted in Figure 1, in
126 accord with our past studies (Rhoades et al. 2015; Huang et al. 2016; Huang and Ullrich 2016).

127 Simulations have been performed for the historical period (1979-2005, hereafter referred to as
128 `hist`) and for two future periods: 2024-2050 (hereafter referred to as `mid`) and 2074-2100 (hereafter
129 referred to as `end`). Daily output are recorded for each period on the native SE grid and then
130 remapped to a regional latitude-longitude mesh (??). For purposes of analysis, the first year of
131 each time period was discarded as a spin-up period to allow adequate time for the initialized land
132 and atmosphere to equilibrate. The 26-year duration was chosen to provide an adequate sampling
133 of annual variability for each time phase. As mentioned earlier, GHG concentrations are set based
134 on RCP8.5. Historical SSTs and sea ice are prescribed at 1° resolution, as described by Hurrell
135 et al. (2008). SSTs and sea ice for each future period are developed from fully-coupled RCP 8.5
136 climate simulations with bias correction applied (Cecile Hannay, personal communication). Using
137 prescribed SSTs in place of a coupled ocean model considerably reduces the computation cost and
138 so allows the atmospheric model to be run at a higher overall resolution. Annually-updated land
139 surface datasets, which prescribe land-use characteristics, are interpolated from 0.5° to the land
140 model grid.

141 Ensemble runs are needed to ensure that the sample adequately accounts for climate variability,
142 especially for statistics associated with climatological extremes. However, the exact number of
143 ensemble members required is heavily dependent on the variability of the particular metric being
144 examined, and so no standard ensemble criteria exists. Deser et al. (2012b) suggest that around
145 3 ensemble runs are required to detect a significant epoch difference for JJA (June-July-August)
146 surface temperatures, whereas 10 to 30 ensemble members are needed for that for DJF (Dec.-Jan.-
147 Feb.) precipitation. In our study, the use of prescribed SSTs does reduce the intrinsic variability
148 of the climate system (see supplement), and so we found reasonably converged results with two
149 ensemble members for the historical period and four ensemble members for each future period.

150 **3. Methodology**

151 *a. Precipitation indices*

152 Standard indices have been employed to characterize precipitation (Tebaldi et al. 2006; Zhang
153 et al. 2011; Sillmann et al. 2013). In order to choose a comprehensive (but minimal) set that are
154 informative to stakeholders and water managers, indices from throughout the literature have been
155 assessed. The indices examined include those defined by the Expert Team on Climate Change De-
156 tection and Indices (ETCCDI) (Karl et al. 1999) that are featured in earlier studies (Dulière et al.
157 2011; Sillmann et al. 2013; Diffenbaugh et al. 2005; Singh et al. 2013) and others such as return
158 levels, dry spell and wet spell characteristics defined by either percentiles or by selected thresh-
159 olds. The indices we have chosen for this study attempt to provide a relatively comprehensive
160 characterization of precipitation, and are summarized in Table 1.

161 [Paul: You should probably state at some point why you don't employ drought or dry spell
162 indices]

163 *b. Impacts of ENSO*

164 The impact of ENSO on precipitation is emphasized in our study due to its influence on precipi-
165 tation over a majority of our study area, particularly the southwest U.S. (Cayan et al. 1999; Zhang
166 et al. 2010; Deser et al. 2012a; Yoon et al. 2015). The phase of ENSO (*i.e.* El Niño and La Niña)
167 is identified each year using the Oceanic Niño Index (ONI), defined as the 3-month running means
168 of SST anomalies in the Niño 3.4 region (covering 5N-5S, 120-170W based on NOAA (2013)).
169 An El Niño or La Niña episode is said to occur when the ONI exceeds +0.5 or -0.5 for at least five
170 consecutive months for a water year (*i.e.* from July to June) (NOAA 2013) (see the supplement).
171 In order to adjust for the trend in the SST field associated with climate change, the anomaly is

172 computed against the detrended mean SSTs from the periods 1971-2000, 2020-2050 and 2070-
173 2100 for hist, mid and end respectively, using the aforementioned observed and predicted SST
174 datasets. As argued by Kao and Yu (2009), it may be desirable to use an extended Niño 3.4 region
175 to determine the phase of ENSO – however, when employing SST anomalies integrated over the
176 region 105-170W, we observed no significant impact on ONI statistics.

177 *c. Assessing significance*

178 Student's t-test has been used to test whether or not two datasets at each grid point are statisti-
179 cally equivalent, if the sample population can be adequately described by a normal distribution.
180 The normality of a dataset is assessed under the Anderson-Darling test. When the sample popu-
181 lations do not approximately follow a normal distribution, Mann-Whitney-Wilcoxon (MWW) test
182 is employed in lieu of the t-test. All these tests are evaluated at the 0.05 (α) significance level.
183 Among different time periods, those statistical tests are conducted using all the yearly values of
184 each ensemble run.

185 (add description of the supplement like what are included; see the sst_enso.pdf, mask the land
186 (over land, it should the surface temperature.))

187 *d. Reference datasets*

188 Gridded observational datasets and reanalysis of the highest available quality with comparable
189 horizontal resolutions to our VR-CESM simulations are used for assessing the simulation qual-
190 ity. The use of multiple reference datasets is necessary due to the underlying uncertainty in the
191 reference data. Descriptions of the datasets employed are as follows.

192 **UW Precipitation Dataset:** The UW daily gridded meteorological data is obtained from the
193 Surface Water Modeling group at the University of Washington (Maurer et al. 2002; Hamlet

194 and Lettenmaier 2005). UW incorporates topographic corrections for the precipitation. The
195 dataset is provided at 0.125° horizontal resolution covering the period 1949 to 2010.

196 **NCEP CPC:** This dataset provides gauge-based analysis of daily precipitation from the Na-
197 tional Oceanic and Atmospheric Administration (NOAA) Climate Prediction Center (CPC).
198 It is a suite of unified precipitation products obtained by combining all information avail-
199 able at CPC via the optimal interpolation objective analysis technique. The gauge analysis
200 covers the Conterminous United States with a fine-resolution at 0.25° from 1948-01-01 to
201 2006-12-31.

202 **North American Regional Reanalysis (NARR):** The is the NCEP (National Centers for En-
203 vironmental Prediction) high-resolution reanalysis product that provides dynamically down-
204 scaled data over North America at ~ 32 km resolution and 3-hourly intervals from 1979
205 through present (Mesinger et al. 2006).

206 4. Model Assessment

207 Before proceeding, we first investigate how well the model is able to represent the character
208 of precipitation over the WUS. Figures 2 and Figure 3 depict the spatial character of the indices
209 defined in Table 1. Considering the uncertainty within the reference datasets, the mean of the ref-
210 erences are used to get the difference from the model output. T-test is applied here with UW, CPC
211 and NARR as the three statistical samples and the historical runs as two samples averaged over
212 the whole period, determining at each spatial point whether VR-CESM is statistically equivalent
213 to the references as stippled in 2 and 3.

214 Compared with observations, VR-CESM well represents the spatial pattern of precipitation, with
215 majority of the precipitation distributed along the northwest coastal area and the mountainous re-

216 gions of the Cascades and the Sierra Nevada. Compared to the mean of the references, VR-CESM
217 does overestimate the Pr significantly over most of the relatively dry region for about 0.2 mm to
218 1.5 mm, especially over the eastern side of the Cascades and both sides of the Sierra Nevada (with
219 relatively difference reaching 50%-150%). This is further reflected in the overestimation of the
220 non-extreme Pr events frequency (with $Pr = <10\text{mm/day}$) since most precipitation over dry area
221 is associated with low rainy rate days. However, for the western flank of the Sierra Nevada, the
222 overestimation of the mean Pr is mainly due to the intensified rain rate, which may related with
223 the strengthened treatment of orographic effects with excessively strong upward winds. Nonethe-
224 less, the model captures the precipitation features including frequency and intensity satisfactorily
225 over the main wet region, where most precipitation is resulted from extreme Pr events (when
226 $Pr > 10\text{mm/day}$), without significant difference.

227 The corresponding contribution fraction to total precipitation amount of each range defined in
228 our metrics is also well represented in the model without significant difference, except the western
229 side of the the Sierra Nevada and eastern flank of the Cascades in the Washington. This suggests
230 that despite the aforementioned biases, VR-CESM can still capture the overall shape of the precip-
231 itation distributions. Biases in simulating extreme precipitation over the topographically complex
232 regions including the Cascades and Sierra Nevada ranges have also been found by in the high-
233 resolution simulation by RCMs Walker and Diffenbaugh (2009); Singh et al. (2013), and have
234 been primarily attributed to excessively strong winds. Biases with the excessively dry eastern
235 flanks of these mountains may also be associated with the diagnostic treatment of precipitation
236 species in CESM.

237 As further supported in Huang et al. (2016) by evaluating VR-CESM also at 0.25° for long-term
238 regional climate modeling over California, it is found that VR-CESM can adequately represented
239 regional climatological patterns with high spatial correlations. VR-CESM shows comparable per-

240 formance as WRF at 27 km, but still overestimated overall winter precipitation (about 25%-35%)
241 compared to reference datasets, with statistically significant difference over the western edge of
242 the Sierra Nevada. **This bias is not alleviated by simply increasing the spatial resolution, as it still**
243 **exists when refining this region down to 4km (Alan M. Rhoades, personal communication), sug-**
244 **gesting that the bias might be related with more complex dynamic processes rather than treatment**
245 **of the orographic effects.** The spatial pattern of variability agrees well between VR-CESM and
246 references and when assessing the frequency of strong precipitation events, VR-CESM matched
247 closely to the UW dataset everywhere except the Central Valley.

248 CESM at 1 degree resolution was also assessed in order to better understand the impacts of reso-
249 lution. We find that precipitation patterns over complex topography are poorly represented without
250 capturing the spatial patterns induced by orographic effects over the Cascades and Sierra Nevada
251 by uniform CESM at 1 degree, with total precipitation greatly underestimated, when compared to
252 VR-CESM, gridded data and reanalysis (see the supplement). Basically, the precipitation has been
253 smooth out at the coastal area and the mountainous regions over northwest U.S when simulated
254 with CESM at coarse resolution. This result clearly captures the benefits of high resolution (par-
255 ticularly the representation of topography) in simulating precipitation features. Results are also
256 provided for the output from a globally uniform CESM run at 0.25° spatial resolution with the
257 finite volume (FV) dynamical core (Wehner et al. 2014), exhibiting comparable performance to
258 VR-CESM (see the supplement).

259 We have also assessed the ENSO effect modeled by VR-CESM identified by the difference of
260 precipitation behaviors between the warm phase (i.e. El Niño) and cool phase (i.e. La Niña)
261 of ENSO, compared to references (see the supplement). The impact of ENSO for observational
262 precipitation has a weaker signal compared to the VR-CESM, which might suggest that the model
263 has an overestimation of ENSO's impact on precipitation, especially over the northwest U.S. The

264 improvement of ENSO in the model is directly proportional to the representation of ENSO forced
265 precipitation anomalies (AchutaRao and Sperber 2006).

266 **5. Drivers of climatological precipitation**

267 Precipitation has been observed and modeled to being changed both regionally and globally
268 under climate warming as discussed in the introduction. The observed intensification of heavy
269 precipitation events over the the latter half of the twentieth century is attributed to the human-
270 induced increases in GHGs over majority of Northern Hemisphere land areas (Min et al. 2011),
271 although no significant changes in the total precipitation has been observed globally (Donat et al.
272 2016). With the coupled effects of continued increasing CO₂ and SSTs in the future, precipitation
273 is assumed to be changed driven by both the radiative changes in the lower troposphere and inten-
274 sified water vapor evaporation over the ocean (Allen and Ingram 2002; Sugi and Yoshimura 2004).
275 Precipitation extremes are projected to intensify continuously through the end of 21st century in
276 both dry and wet regions with heterogeneous patterns (Donat et al. 2016).

277 As described by the Clausius-Clapeyron (C-C) equation, the water vapor content is supposed
278 to increase by ~7% for each 1°C increase in temperature (Allan and Soden 2008). Naturally,
279 evaporation over the ocean will increase with the climate warming, but the increasing rate may be
280 constrained over land due to limitations by soil moisture (Cayan et al. 2010). When the air holds
281 more water vapor, the chances of heavy rain events tend to increase even at which total precipita-
282 tion is decreasing (Trenberth 2011), given that global total precipitation is expected to increase at
283 a lower rate than precipitation extremes (Allan and Soden 2008). According to previous studies
284 (e.g. (Allan and Soden 2008; O'Gorman and Schneider 2009; Min et al. 2011)), changes in more
285 extreme precipitation follow the C-C relationship more closely than total precipitation amount
286 (Trenberth et al. 2003). However, those changes are still remain uncertain with the increasing rate

287 of precipitation extremes affected by multiple factors including the vertical velocity profile and
288 temperature changes (O’Gorman and Schneider 2009).

289 The moderate or heavy precipitation events over WUS mainly result from the large-scale water
290 flux transport from the eastern Pacific Ocean rather than directly from evaporation, usually in
291 the form of atmospheric rivers (ARs) or orographic updraft (Trenberth et al. 2003; Neiman et al.
292 2008). The storm track may be enhanced, which would increase ARs along the U.S. west coast
293 with increased air water vapor content in the future (Dettinger 2011; Gao et al. 2015). In the
294 following section, both the mean changes of precipitation and distributions of both non-extreme
295 and extreme events are investigated as projected by the VR-CESM model under an extreme climate
296 forcing context(i.e. RCP 8.5).

297 The precipitation of WUS has strong inter-annual variability caused by large-scale atmospheric
298 circulation mainly associated with the ENSO (Leung et al. 2003b). As a significant driver
299 of precipitation, ENSO modulates the storm track behavior over western U.S. with a north-
300 west/southwest precipitation dipole (Gershunov and Barnett 1998), as discussed in 2. The pro-
301 jected SSTs we used here states one of the possible cases of ENSO scenarios in the future. How-
302 ever, there is still substantial uncertainty regarding how El Niño will change under global warming
303 (Fedorov and Philander 2000; Guilyardi et al. 2009), resulting corresponding uncertainty in our
304 results. Capotondi (2013) showed that the diversity of El Niño characteristics in CCSM4 is com-
305 parable to what was found in observations, although, as found by Deser et al. (2012c), the overall
306 magnitude of ENSO in CCSM4 is overestimated by 30% over the preindustrial time period.

307 **6. Results**

308 *a. Mean climatology*

309 Before proceeding with the analysis of precipitation features, it is first important to understand
310 how the mean climatology changes in VR-CESM across time periods (Figure 4). Since the charac-
311 ter of WUS precipitation has a strong seasonal dependence, the mean climatology including mean
312 precipitation, near-surface temperature and near-surface relative humidity are depicted in two sea-
313 sons including the cool season (or wet season) from October to March and the warm season (or
314 dry season) from April to September.

315 As a result of enhanced GHG concentrations, mean annual near-surface temperature (T2avg)
316 increases by about 1.5 to 2 K from hist to mid and about 4 to 6 K from mid to end. Despite the
317 large spatial variation in climatological temperatures, the temperature change between historical
318 and future is fairly uniform. However, there is a slightly weaker increase in the near-coastal
319 regions during cool season and in the lower latitude area at warm season, which might be due to
320 the increased westerly wind during cool seasons and northward wind during warm season from
321 the near ocean. Larger increases of temperature is also observed in warm season than cool season
322 for about 0.5 K and 1 K for mid and end respectively.

323 Practically, whether the increase rate of the water vapor as the temperature goes up will keep the
324 same or not will directly affect the relative humidity. As water vapor reaches saturation, conden-
325 sation triggers clouds and precipitation. To understand the increasing rate of water vapor content
326 under climate warming and whether relative humidity can be remain or not, 2m relative humidity
327 (RH) is plotted in Figure 4.

328 Overall, RH remains almost the same as hist over the regions where temperature does not sub-
329 stantially increase. However, in regions where temperature increase is larger than 2 K, RH is

330 instead observed to decrease significantly relative to historical values for about 2% and 3-6%
331 compared to mid and end respectively. In fact, trends in RH are spatially consistent with tempera-
332 ture increase but opposite in magnitude with a spatial correlation coefficient of approximately 0.8.
333 RH still remains the same or increase over part of the near-coastal area over the Pacific Ocean due
334 to the lower increase of T2avg compared to the land area. This suggests that continental evapo-
335 ration and oceanic water vapor transport are insufficient to compensate for the air vapor capacity
336 when temperature increases to certain level, which is consistent with Joshi et al. (2008), and has
337 been observed in results by Rowell and Jones (2006) over continental and southeastern Europe
338 and Simmons et al. (2010) over low-latitude and midlatitude land areas.

339 Based on those background changes of heat and water vapor, from hist to mid, mean precipita-
340 tion showed a 0.2-0.6 mm/day increase during cool season with a largest change over northwest
341 and less than 0.2 mm/day during warm season over southeast part. From hist to end, the increase is
342 about 0.4-1.2 mm/day during cool season with also a largest change over northwest, and no notable
343 change is observed during warm season. Nonetheless, these results are statistically significant (see
344 Figure 5). East of the Rockies, precipitation increases through mid-century (statistically signifi-
345 cant), but this trend appears to recede towards the end of the century (although these results are not
346 significant). There is also a decrease of about 0.1mm/day in total precipitation over the western
347 flank of the Sierra Nevadas during the cool season from hist to future. This decrease (about 0.15
348 mm/day) is also found over the Cascades and the western coastal area during warm season from
349 hist to mid. However, this decrease is not statistically significant. Majority of the precipitation
350 over the cool season emerged from large-scale patterns, whereas warm season precipitation was
351 from convection processes. The precipitation over WUS for moderate or heavy precipitation is
352 mainly due to the large-scale water flux transport from the eastern Pacific Ocean rather than di-

353 rectly from evaporation, mainly in the form of atmospheric rivers or orographic updraft (Trenberth
354 et al. 2003; Neiman et al. 2008).

355 The increase of mean wet season precipitation over the northwest is mainly caused by the en-
356 hanced orographic precipitation due to increased integrated vapor transport (IVT). The IVT in-
357 creases due to higher water vapor content from increased ocean evaporation, which is affected pri-
358 marily by climatological forcing. Over southern California, precipitation did not show significant
359 changes since no substantial increase in IVT over Eastern Pacific Ocean near southern California
360 coast is predicted, with IVT in this region driven primarily by variations in ENSO. Since pre-
361 cipitation over the Intermountain West during warm season is mainly results from the convection
362 processes, precipitation is directly related with the changes of the relative humidity. As shown
363 in Figure 4, RH has decreased over most the study area except over where the soil moisture is
364 relatively low when going to end. Further, the changes of RH are related with the soil moisture
365 magnitude accompanying the changes of latent heat flux during warm season.

366 According to previous studies (e.g. (Allen and Ingram 2002; Allan and Soden 2008; O’Gorman
367 and Schneider 2009; Min et al. 2011)), changes in more extreme precipitation follow the C-C
368 relationship more closely than total precipitation amount (Trenberth et al. 2003).
369 In order to find out the precipitation changes in a comprehensive aspect based on our fine-scale
370 simulations, analyses of different precipitation distributions are focused in the following part to
371 account for the future changes of diverse precipitation events.

372 *b. Precipitation indices*

373 To see how precipitation changes in a comprehensive way, we have analyzed detailed precipita-
374 tion distributions in order to account for the future changes of different precipitation events, based
375 on our simulation results. The precipitation indices are presented in Table 1. For each index, the

376 changes of precipitation character for each period, averaged over all ensemble members are plotted
377 in Figure 5 (for the indices that quantify precipitation days) and Figure 6 (for the indices describing
378 precipitation amounts). Although mean precipitation shows a weak but overall increasing trend
379 from hist to mid and mid to end (about 10-15%), the precipitation indices exhibit substantially
380 more unique character.

381 When comparing hist to mid, the total rainy days and frequency of non-extreme precipitation
382 have significantly increased (about 10-15%) mainly over the central-east and southeast part of
383 WUS, which is less obvious between mid and end. On the contrary, the frequency of non-extreme
384 precipitation have decreased significantly over the northwest region and the eastern part of the
385 Montana, Wyoming and Oregon from mid to end (about 10%). These changes are the primary
386 driver for the observed change to mean precipitation exhibited in Figure 4.

387 As for extreme precipitation frequency (i.e. days with daily Pr between 10 mm and 40 mm), the
388 number of days increases from hist to mid, but the pattern is scattered over northwest and central
389 WUS. When comparing mid to end, there is a clear and significant increase in extreme precip-
390 itation events over the northwest coastal area (about 20-30%) and eastern flank of the Cascades
391 (larger than 40%). This result is consistent with Dominguez et al. (2012), who observe a robust
392 increase in winter precipitation extremes toward the latter half of the 21st century by an ensemble
393 of RCMs. There is a slight, but insignificant decrease over the Cascades and the Sierra Nevada
394 (significance is low due to the high variability of precipitation). No notable predicted changes have
395 been observed over California.

396 The associated precipitation signal under a warmer climate is more ambiguous for California
397 (Neelin et al. 2013) considering the extreme variability on interannual time scales (Dettinger
398 2011). Kim (2005) found that under global warming, heavy precipitation events show largest
399 increases in the mountainous regions of the northern California Coastal Range and the Sierra

400 Nevada. However, our results show a minor decrease (though not statistically significant) of ex-
401 treme precipitation over the Sierra Nevada. The decrease over southwest U.S. is mainly due to the
402 intensified La Niña in the future as shown in the Section 2.

403 For very extreme precipitation ($\text{Pr} \geq 40 \text{ mm}$) events, there is an increasing trend over the north-
404 west coast (larger than 60%) and the Cascades (about 50%) and its eastern flank (larger than 60%)
405 when comparing `hist` to `end`. Significant changes have also observed over the northern moun-
406 tainous part of California for about 20-40% from `hist` to `end`. The corresponding changes in rain
407 amount are consistent with the changes of frequency (see Figure 6). Overall, these results indi-
408 cate more extreme precipitation over the northwest U.S with changes in precipitation extremes
409 following more consistently with the C-C relationship.

410 In order to understand the drivers behind the observed changes, we first examine change in
411 moisture flux for cool seasons when WUS precipitation is primarily from water vapor influx from
412 the Pacific Ocean (see Figure 7). We observe an increase in specific humidity at 850 hPa that
413 accompanies the increase of the temperature in future. **However, when comparing to `hist`, westerly**
414 **wind tends to weaken in mid and end over the eastern part of the WUS and strengthen over western**
415 **area.**

416 IVT (Figure 7) for extreme precipitation days over cool seasons. Generally, IVT is useful to
417 understand extreme precipitation events that arise from atmospheric rivers over the northwestern
418 U.S. and from orographic uplift (especially for very extreme precipitation) (Ralph et al. 2004;
419 Leung and Qian 2009; Dettinger 2011). Based on the observed change in IVT, it is clear that the
420 increase in moisture influx from past to future, which is mainly due to the change of the air water
421 vapor content with increased temperature, corresponds to the changes of precipitation extremes
422 shown in Figure 5.

423 1) QUANTILE CORRELATION ANALYSIS

424 To see if changes in mean precipitation can be used to predict changes in extreme precipitation
425 features, the correlations between Pr and specific quantiles have been calculated. Here, selected
426 quantiles including the values at 70% (70p), 80% (80p), 90% (90p), 95% (95p) and 99% (99p)
427 are applied based on the all the daily precipitation data at each grid point within each time period.
428 These quantiles are chosen in order to account for the changes of both moderation and extreme
429 precipitation. The mean Pr and those quantiles for hist, and the differences of these quantities
430 among different time periods can be found in the supplemental figure. Within expectation, regions
431 with higher Pr are associated with larger values of those quantiles, i.e. stronger precipitation
432 extremes. This is further supported by the high correlation (about 0.7-0.9) between Pr and R20mm,
433 R40mm, and Rxmm, not between Pr and non-extreme precipitation events.

434 Spatial correlation is assessed by computing Pearson product-moment coefficient of linear corre-
435 lation between relevant variables. It is found that the absolute changes of Pr in future are positively
436 related with the absolute changes of the quantiles. This relationship is at a moderate level between
437 mid and hist (larger than 0.65), and becomes stronger when going to the end period (reaching
438 ~0.96). Consistently, the mean Pr itself is also positively correlated with the absolute changes of
439 the quantiles in future (around 0.5 to 0.78), except 70p between end and mid and 99p mid and
440 hist.

441 The relative changes of quantiles are also related with the relative changes of Pr with correla-
442 tions around 0.65 to 0.85, except 70p and 80p between end and mid. So, the area featured with
443 higher increase of extreme precipitations in future also tends to have larger increase of its mean
444 precipitation. However, the wetter area does not necessary have more intense changes of moder-
445 ate and extreme precipitation than drier area. [The changes of Pr is not obviously correlated with](#)

⁴⁴⁶ the changes of precipitation indices, which further states that mean precipitation and precipitation
⁴⁴⁷ events undergo different features of changing in the future.

⁴⁴⁸ might divide into four regions; PDF of each region? [Paul: This is a good idea]

⁴⁴⁹ 2) ISOLATING DIFFERENCES DUE TO CLIMATE CHANGE AND ENSO

⁴⁵⁰ The phase of ENSO is well known to have important repercussions on precipitation extremes
⁴⁵¹ (Larkin and Harrison 2005; Allan and Soden 2008; Maloney et al. 2014; Yoon et al. 2015). Cai
⁴⁵² et al. (2014) found a significantly increase for extraordinary precipitation along the eastern Pacific
⁴⁵³ Ocean in the 21st century within the CMIP5 ensemble, associated with increasing frequency of
⁴⁵⁴ extreme El Niño events due to greenhouse warming. In this part, we will figure out how the ENSO
⁴⁵⁵ impacts specific regions over our study area, and whether the effects pattern will change over time.

⁴⁵⁶ ENSO from past to future, the difference of precipitation behaviors between the warm phase (i.e.
⁴⁵⁷ El Niño) and cool phase (i.e. La Niña) of ENSO is illustrated in Figure 8 for the wet seasons of
⁴⁵⁸ each time period. Based on the ONI index values, the mean SST anomalies are 1.38, 1.71 and 2.30
⁴⁵⁹ K during El Niño years, and -1.16, -1.62 and -1.43 K during La Niña years for hist, mid and end
⁴⁶⁰ respectively. The mean SSTs over the Niño 3.4 region where the are 26.83, 28.62 and 30.54°C
⁴⁶¹ for textsfhist, mid and end respectively. Based on the SST datasets we used here, the anomaly
⁴⁶² of ENSO has intensified. The SST anomalies of each year and each month, and their associated
⁴⁶³ spatial pattern when averaged during the warm and cool phases can be found in the supplement,
⁴⁶⁴ exhibiting the increasing frequency of El Niño during for mid and almost doubled frequency of La
⁴⁶⁵ Niña during mid and end compared to the hist.

⁴⁶⁶ (Huang: As SSTs increase in the future, is not it normal for the anomaly of ENSO to be increased
⁴⁶⁷ to compensate the changes of water vapor capacity? Might email Neale about this.)

468 During the El Niño phase, intensified mean precipitation is expected over the southwest (Ham-
469 let and Lettenmaier 2007), along with reduced precipitation intensity over the northwest. In La
470 Niña phase, the pattern is essentially reversed, with wetter conditions in the northwest and a drier
471 situation in the Southwest. This feature is characterized as a northwest/southwest precipitation
472 dipole, triggered by ENSO's modification of the storm track (Gershunov and Barnett 1998; Le-
473 ung et al. 2003b), along with modulation of the enhanced precipitation variability (Cayan et al.
474 1999; Kahya and Dracup 1994). This dipole is also apparently in the frequency of rainy days and
475 extreme precipitation events.

476 In mid and hist, ENSO is observed to intensify, which appears to be related with the changes
477 of the strength of El Niño and La Niña. This can be explained by the SST anomaly magnitude
478 (detrended) of warm and cold phases (see the supplement). DeFlorio et al. (2013) also found a
479 statistically significant linkages with ENSO and PDO for both the overall and extreme intensity
480 of wintertime precipitation over the WUS using CCSM4 (earlier form of CESM). Strengthening
481 storm patterns associated with ENSO are also found by Maloney et al. (2014) over California using
482 CMIP5 output under RCP8.5.

483 We have also checked the teleconnection effect of Pacific Decadal Oscillation (PDO) and it
484 did not show strong effect alone. Precipitation features did not change notably when at the cool
485 phase or warm phase of PDO during hist. However, together with ENSO at the same phase,
486 PDO can have notable effect over northwest. This coupled effect has been found by previous
487 studies Gershunov and Barnett (1998), stating ENSO and PDO can "reinforce" each other with
488 PDO responding to the same internal atmospheric variability as ENSO (Pierce 2002). **In our**
489 **simulations, the patterns of PDO phases differs quite a bit from past to future, though there were**
490 **roughly an equal number of positive PDO years and negative PDO years in the data. We suppose**

491 that our 26 years simulation time period might not be long enough to account for the variability of
492 PDO due to its duration for decades. Therefore, in this study, the PDO is not specifically analyzed.

493 The impact of ENSO is further observed by the IVT difference over rainy days between El Niño
494 and La Niña (see Figure 9) accompanying by the wind pattern difference at 850 hPa, showing the
495 increase of the moisture flux for the southwest and decrease for the northwest. This suggests the
496 major role of moisture influx regulation of ENSO.

497 Based on the above results, it can be seen that the magnitude of the effects of ENSO is compara-
498 ble or even higher than the impacts of climate forcing. For further investigation, linear regression
499 is applied to signaling the factor effects due to ENSO and climate forcing. First, we get the SST
500 anomaly of each cool season when ENSO mainly affect followed by the way of Niño 3.4 to be
501 the ENSO factor values. Then, we use the GHGs values at each year to represent the climate
502 forcing factor. The features of the precipitation indices as we defined above are used as response
503 variables. Combined the values of all the time period and all the runs, we got the significance of
504 these two factors' effects at each grid point based on the ANOVA (analysis of variance) output
505 (see the supplement). Changing of the SSTs anomaly can affect most of the study area for non-
506 extreme precipitation events, and southern regions and the Cascades and the Rocky Mountains for
507 precipitation extremes. The GHGs factor mainly shows significant impacts over the northwest and
508 inter-mountainous regions for both non-extreme and extreme precipitation events.

509 We have also examined the linear coefficients of these two factors over where their effects are
510 significant to see the strength that ENSO and GHGs play at each grid point (see the supplement). It
511 is found that the effect of the ENSO is similar to the pattern of the difference between El Niño and
512 La Niña (see Figure 9). In contrast, the effect of the GHGs is close to the pattern of the difference
513 between the different time periods (see Figure 5). We do acknowledge that the values might not be
514 accurate due to the simple linear mode we used here. However, the qualitative conclusions won't

515 change. Therefore, we assume that even the ENSO largely regulates the precipitation over different
516 phases, it won't affect our results shown here for the changes of precipitation features from past to
517 future. Although here is just one of the possible cases of ENSO scenarios in the future, as ENSO
518 behavior is strongly dependent on choice of climate models, the underlying principles should still
519 be consistent.

520 Although, the strength of ENSO intensifies in the future with CESM, there is still substantial
521 uncertainty regarding how El Niño will change under global warming as debated by plenty of
522 studies (Fedorov and Philander 2000; Guilyardi et al. 2009), particularly as ENSO appears to be
523 relatively insensitive to a doubling of CO₂ in most models (DiNezio et al. 2012). Correctly simula-
524 tion changes to the spatial pattern of SSTs ion state-of-the-art coupled GCMs remains challenging
525 Joseph and Nigam (2006); ?); Jha et al. (2014); Taschetto et al. (2014).

526 **7. Discussion and Summary**

527 The increased cool season precipitation extremes tend to result in higher runoff events over
528 the northwest U.S., which are in turn associated with a greater chance of flooding and a loss of
529 snowpack. A decrease in counts of rainy days during the warm season over central and southern
530 California, though small in magnitude, will probably intensify the drought condition due to the
531 deficit of soil moisture with higher evapotranspiration caused by the warmer climate in the future
532 Cayan et al. (2010); Bell et al. (2004).

533 (Huang: Yoon et al. (2015) found a strengthened relation with ENSO for the projected increase
534 in water cycle extremes in California using the output from CESM1 and CMIP5. Similarly by
535 Maloney et al. (2014) using CMIP5 dataset. (check the CESM1?))

536 (Summary is to be added once the main content have been settled down The contribution of
537 human-induced increases in greenhouse gases to the character of precipitation is confounded by

538 patterns of variability in the atmospheric circulation. Consistent with previous studies, changes
539 in more extreme precipitation follow the Clausius-Clapeyron relationship more closely than total
540 precipitation amount. The changes of the strength of ENSO remains uncertain. However, the char-
541 acter of ENSO appears to be the largest factor in understanding changing precipitation extremes
542 in the U.S. West.)

543 *Acknowledgments.* The authors would like to thank Michael Wehner for sharing the dataset and
544 many suggestions. The authors also want to thank Alan M. Rhoades for providing the simulation
545 output. We acknowledge the substantial efforts behind the datasets used in this study, including
546 UW, NCDC and NARR. The simulation data used is available by request at xyhuang@ucdavis.edu.
547 This project is supported in part by the xxx and by the xxx.

548 References

- 549 AchutaRao, K., and K. R. Sperber, 2006: Enso simulation in coupled ocean-atmosphere models:
550 are the current models better? *Climate Dynamics*, **27** (1), 1–15.
- 551 Allan, R. P., and B. J. Soden, 2008: Atmospheric warming and the amplification of precipitation
552 extremes. *Science*, **321** (5895), 1481–1484.
- 553 Allen, M. R., and W. J. Ingram, 2002: Constraints on future changes in climate and the hydrologic
554 cycle. *Nature*, **419** (6903), 224–232.
- 555 Bell, J. L., L. C. Sloan, and M. A. Snyder, 2004: Regional changes in extreme climatic events: a
556 future climate scenario. *Journal of Climate*, **17** (1), 81–87.
- 557 Cai, W., and Coauthors, 2014: Increasing frequency of extreme el niño events due to greenhouse
558 warming. *Nature climate change*, **4** (2), 111–116.

- 559 Caldwell, P., 2010: California wintertime precipitation bias in regional and global climate models.
- 560 *Journal of Applied Meteorology and Climatology*, **49** (10), 2147–2158.
- 561 Capotondi, A., 2013: Enso diversity in the ncar ccm4 climate model. *Journal of Geophysical*
- 562 *Research: Oceans*, **118** (10), 4755–4770.
- 563 Cayan, D. R., T. Das, D. W. Pierce, T. P. Barnett, M. Tyree, and A. Gershunov, 2010: Future
- 564 dryness in the southwest us and the hydrology of the early 21st century drought. *Proceedings of*
- 565 *the National Academy of Sciences*, **107** (50), 21 271–21 276.
- 566 Cayan, D. R., K. T. Redmond, and L. G. Riddle, 1999: ENSO and hydrologic extremes in the
- 567 western United States*. *Journal of Climate*, **12** (9), 2881–2893.
- 568 DeFlorio, M. J., D. W. Pierce, D. R. Cayan, and A. J. Miller, 2013: Western us extreme precipita-
- 569 tion events and their relation to enso and pdo in ccm4. *Journal of Climate*, **26** (12), 4231–4243.
- 570 Dennis, J., and Coauthors, 2011: CAM-SE: A scalable spectral element dynamical core for the
- 571 Community Atmosphere Model. *International Journal of High Performance Computing Appli-*
- 572 *cations*, 1094342011428142.
- 573 Deser, C., R. Knutti, S. Solomon, and A. S. Phillips, 2012a: Communication of the role of natural
- 574 variability in future north american climate. *Nature Climate Change*, **2** (11), 775–779.
- 575 Deser, C., A. Phillips, V. Bourdette, and H. Teng, 2012b: Uncertainty in climate change projec-
- 576 tions: the role of internal variability. *Climate Dynamics*, **38** (3-4), 527–546.
- 577 Deser, C., and Coauthors, 2012c: Enso and pacific decadal variability in the community climate
- 578 system model version 4. *Journal of Climate*, **25** (8), 2622–2651.
- 579 Dettinger, M., 2011: Climate change, atmospheric rivers, and floods in california—a multimodel
- 580 analysis of storm frequency and magnitude changes1. Wiley Online Library.

- 581 Diffenbaugh, N. S., J. S. Pal, R. J. Trapp, and F. Giorgi, 2005: Fine-scale processes regulate the
582 response of extreme events to global climate change. *Proceedings of the National Academy of*
583 *Sciences of the United States of America*, **102** (44), 15 774–15 778.
- 584 DiNezio, P. N., B. P. Kirtman, A. C. Clement, S.-K. Lee, G. A. Vecchi, and A. Wittenberg, 2012:
585 Mean climate controls on the simulated response of enso to increasing greenhouse gases. *Journal*
586 *of Climate*, **25** (21), 7399–7420.
- 587 Dominguez, F., E. Rivera, D. Lettenmaier, and C. Castro, 2012: Changes in winter precipitation
588 extremes for the western united states under a warmer climate as simulated by regional climate
589 models. *Geophysical Research Letters*, **39** (5).
- 590 Donat, M. G., A. L. Lowry, L. V. Alexander, P. A. OGorman, and N. Maher, 2016: More extreme
591 precipitation in the world [rsquor] s dry and wet regions. *Nature Climate Change*.
- 592 Duffy, P., and Coauthors, 2006: Simulations of present and future climates in the western United
593 States with four nested regional climate models. *Journal of Climate*, **19** (6), 873–895.
- 594 Duli re, V., Y. Zhang, and E. P. Salath  Jr, 2011: Extreme Precipitation and Temperature over the
595 US Pacific Northwest: A Comparison between Observations, Reanalysis Data, and Regional
596 Models*. *Journal of Climate*, **24** (7), 1950–1964.
- 597 Easterling, D. R., G. A. Meehl, C. Parmesan, S. A. Changnon, T. R. Karl, and L. O. Mearns, 2000:
598 Climate extremes: observations, modeling, and impacts. *science*, **289** (5487), 2068–2074.
- 599 Fedorov, A. V., and S. G. Philander, 2000: Is el ni o changing? *Science*, **288** (5473), 1997–2002.
- 600 Fox-Rabinovitz, M., J. C te, B. Dugas, M. D qu , and J. L. McGregor, 2006: Variable resolution
601 general circulation models: Stretched-grid model intercomparison project (SGMIP). *Journal of*
602 *Geophysical Research: Atmospheres (1984–2012)*, **111** (D16).

- 603 Fox-Rabinovitz, M. S., G. L. Stenchikov, M. J. Suarez, and L. L. Takacs, 1997: A finite-
604 difference GCM dynamical core with a variable-resolution stretched grid. *Monthly weather*
605 *review*, **125** (11), 2943–2968.
- 606 Frei, C., R. Schöll, S. Fukutome, J. Schmidli, and P. L. Vidale, 2006: Future change of precipita-
607 tion extremes in Europe: Intercomparison of scenarios from regional climate models. *Journal*
608 *of Geophysical Research: Atmospheres (1984–2012)*, **111** (D6).
- 609 Gao, Y., J. Lu, L. R. Leung, Q. Yang, S. Hagos, and Y. Qian, 2015: Dynamical and thermodynami-
610 cal modulations on future changes of landfalling atmospheric rivers over western north america.
611 *Geophysical Research Letters*, **42** (17), 7179–7186.
- 612 Gates, W. L., 1992: AMIP: The Atmospheric Model Intercomparison Project. *Bulletin of the*
613 *American Meteorological Society*, **73**, 1962–1970.
- 614 Gershunov, A., and T. P. Barnett, 1998: Interdecadal modulation of enso teleconnections. *Bulletin*
615 *of the American Meteorological Society*, **79** (12), 2715–2725.
- 616 Grodsky, S. A., J. A. Carton, S. Nigam, and Y. M. Okumura, 2012: Tropical atlantic biases in
617 ccesm4. *Journal of Climate*, **25** (11), 3684–3701.
- 618 Guilyardi, E., A. Wittenberg, A. Fedorov, M. Collins, C. Wang, A. Capotondi, G. J. Van Olden-
619 borgh, and T. Stockdale, 2009: Understanding el niño in ocean-atmosphere general circulation
620 models. *Bulletin of the American Meteorological Society*, **90** (3), 325.
- 621 Hamlet, A. F., and D. P. Lettenmaier, 2005: Production of Temporally Consistent Gridded Precipi-
622 tation and Temperature Fields for the Continental United States*. *Journal of Hydrometeorology*,
623 **6** (3), 330–336.

- 624 Hamlet, A. F., and D. P. Lettenmaier, 2007: Effects of 20th century warming and climate variability
625 on flood risk in the western us. *Water Resources Research*, **43** (6).
- 626 Hegerl, G. C., F. W. Zwiers, P. A. Stott, and V. V. Kharin, 2004: Detectability of anthropogenic
627 changes in annual temperature and precipitation extremes. *Journal of Climate*, **17** (19), 3683–
628 3700.
- 629 Huang, X., A. M. Rhoades, P. A. Ullrich, and C. M. Zarzycki, 2016: An evaluation of the vari-
630 able resolution-cesm for modeling california's climate. *Journal of Advances in Modeling Earth*
631 *Systems*.
- 632 Huang, X., and P. A. Ullrich, 2016: Irrigation impacts on california's climate with the variable-
633 resolution cesm. *Journal of Advances in Modeling Earth Systems*.
- 634 Hurrell, J. W., J. J. Hack, D. Shea, J. M. Caron, and J. Rosinski, 2008: A new sea surface temper-
635 ature and sea ice boundary dataset for the Community Atmosphere Model. *Journal of Climate*,
636 **21** (19), 5145–5153.
- 637 Hurrell, J. W., and Coauthors, 2013: The community earth system model: A framework for col-
638 laborative research. *Bulletin of the American Meteorological Society*, **94** (9), 1339–1360.
- 639 Jha, B., Z.-Z. Hu, and A. Kumar, 2014: Sst and enso variability and change simulated in historical
640 experiments of cmip5 models. *Climate dynamics*, **42** (7-8), 2113–2124.
- 641 Joseph, R., and S. Nigam, 2006: Enso evolution and teleconnections in ipcc's twentieth-century
642 climate simulations: Realistic representation? *Journal of Climate*, **19** (17), 4360–4377.
- 643 Joshi, M. M., J. M. Gregory, M. J. Webb, D. M. Sexton, and T. C. Johns, 2008: Mechanisms for
644 the land/sea warming contrast exhibited by simulations of climate change. *Climate Dynamics*,
645 **30** (5), 455–465.

- 646 Kahya, E., and J. A. Dracup, 1994: The influences of type 1 el nino and la nina events on stream-
flows in the pacific southwest of the united states. *Journal of Climate*, **7 (6)**, 965–976.
- 647
- 648 Kao, H.-Y., and J.-Y. Yu, 2009: Contrasting eastern-pacific and central-pacific types of enso.
649 *Journal of Climate*, **22 (3)**, 615–632.
- 650 Karl, T. R., N. Nicholls, and A. Ghazi, 1999: Clivar/gcos/wmo workshop on indices and indicators
651 for climate extremes workshop summary. *Weather and Climate Extremes*, Springer, 3–7.
- 652 Kharin, V. V., F. W. Zwiers, X. Zhang, and G. C. Hegerl, 2007: Changes in temperature and
653 precipitation extremes in the IPCC ensemble of global coupled model simulations. *Journal of
654 Climate*, **20 (8)**, 1419–1444.
- 655 Kim, J., 2005: A projection of the effects of the climate change induced by increased co2 on
656 extreme hydrologic events in the western us. *Climatic Change*, **68 (1-2)**, 153–168.
- 657 Laprise, R., and Coauthors, 2008: Challenging some tenets of regional climate modelling. *Meteo-
658 rology and Atmospheric Physics*, **100 (1-4)**, 3–22.
- 659 Larkin, N. K., and D. Harrison, 2005: On the definition of el niño and associated seasonal average
660 us weather anomalies. *Geophysical Research Letters*, **32 (13)**.
- 661 Leung, L. R., L. O. Mearns, F. Giorgi, and R. L. Wilby, 2003a: Regional climate research: needs
662 and opportunities. *Bulletin of the American Meteorological Society*, **84 (1)**, 89–95.
- 663 Leung, L. R., and Y. Qian, 2009: Atmospheric rivers induced heavy precipitation and flooding in
664 the western US simulated by the WRF regional climate model. *Geophysical research letters*,
665 **36 (3)**.

- 666 Leung, L. R., Y. Qian, and X. Bian, 2003b: Hydroclimate of the western United States based on
667 observations and regional climate simulation of 1981-2000. Part I: Seasonal statistics. *Journal*
668 *of Climate*, **16 (12)**, 1892–1911.
- 669 Maloney, E. D., and Coauthors, 2014: North american climate in cmip5 experiments: part iii:
670 assessment of twenty-first-century projections*. *Journal of Climate*, **27 (6)**, 2230–2270.
- 671 Maurer, E., A. Wood, J. Adam, D. Lettenmaier, and B. Nijssen, 2002: A long-term hydrologically
672 based dataset of land surface fluxes and states for the conterminous United States*. *Journal of*
673 *climate*, **15 (22)**, 3237–3251.
- 674 McDonald, A., 2003: Transparent boundary conditions for the shallow-water equations: testing in
675 a nested environment. *Monthly weather review*, **131 (4)**, 698–705.
- 676 Meehl, G. A., H. Teng, and G. Bannister, 2006: Future changes of el niño in two global coupled
677 climate models. *Climate Dynamics*, **26 (6)**, 549–566.
- 678 Mesinger, F., and K. Veljovic, 2013: Limited area NWP and regional climate modeling: a test
679 of the relaxation vs Eta lateral boundary conditions. *Meteorology and Atmospheric Physics*,
680 **119 (1-2)**, 1–16.
- 681 Mesinger, F., and Coauthors, 2006: North American regional reanalysis. *Bulletin of the American*
682 *Meteorological Society*, **87**, 343–360.
- 683 Min, S.-K., X. Zhang, F. W. Zwiers, and G. C. Hegerl, 2011: Human contribution to more-intense
684 precipitation extremes. *Nature*, **470 (7334)**, 378–381.
- 685 Neale, R. B., and Coauthors, 2010a: Description of the NCAR community atmosphere model
686 (CAM 5.0). *NCAR Tech. Note NCAR/TN-486+STR*.

- 687 Neale, R. B., and Coauthors, 2010b: Description of the NCAR Community Atmosphere Model
688 (CAM 5.0). NCAR Technical Note NCAR/TN-486+STR, National Center for Atmospheric Re-
689 search, Boulder, Colorado, 268 pp.
- 690 Neelin, J. D., B. Langenbrunner, J. E. Meyerson, A. Hall, and N. Berg, 2013: California winter
691 precipitation change under global warming in the coupled model intercomparison project phase
692 5 ensemble. *Journal of Climate*, **26** (17), 6238–6256.
- 693 Neiman, P. J., F. M. Ralph, G. A. Wick, J. D. Lundquist, and M. D. Dettinger, 2008: Meteorolog-
694 ical characteristics and overland precipitation impacts of atmospheric rivers affecting the west
695 coast of north america based on eight years of ssm/i satellite observations. *Journal of Hydrom-
696 eteorology*, **9** (1), 22–47.
- 697 NOAA, 2013: Defining El Niño and La Niña. Accessed: 2015-
698 08-20, [https://www.climate.gov/news-features/understanding-climate/
699 watching-el-nio-and-la-nia-noaa-adapts-global-warming](https://www.climate.gov/news-features/understanding-climate/watching-el-nio-and-la-nia-noaa-adapts-global-warming).
- 700 O’Gorman, P. A., and T. Schneider, 2009: The physical basis for increases in precipitation ex-
701 tremes in simulations of 21st-century climate change. *Proceedings of the National Academy of
702 Sciences*, **106** (35), 14 773–14 777.
- 703 Oleson, K., and Coauthors, 2010: Technical description of version 4.0 of the Community Land
704 Model (CLM). NCAR Technical Note NCAR/TN-478+STR, National Center for Atmospheric
705 Research, Boulder, Colorado, 257 pp. doi:10.5065/D6FB50WZ.
- 706 Pierce, D. W., 2002: The role of sea surface temperatures in interactions between enso and the
707 north pacific oscillation. *Journal of climate*, **15** (11), 1295–1308.

- 708 Ralph, F. M., P. J. Neiman, and G. A. Wick, 2004: Satellite and caljet aircraft observations of
709 atmospheric rivers over the eastern north pacific ocean during the winter of 1997/98. *Monthly*
710 *Weather Review*, **132** (7), 1721–1745.
- 711 Rauscher, S. A., E. Coppola, C. Piani, and F. Giorgi, 2010: Resolution effects on regional climate
712 model simulations of seasonal precipitation over Europe. *Climate dynamics*, **35** (4), 685–711.
- 713 Rauscher, S. A., T. D. Ringler, W. C. Skamarock, and A. A. Mirin, 2013: Exploring a Global
714 Multiresolution Modeling Approach Using Aquaplanet Simulations. *Journal of Climate*, **26** (8),
715 2432–2452.
- 716 Rhoades, A. M., X. Huang, P. A. Ullrich, and C. M. Zarzycki, 2015: Characterizing Sierra Nevada
717 snowpack using variable-resolution CESM. *Journal of Applied Meteorology and Climatology*,
718 **(2015)**.
- 719 Riahi, K., and Coauthors, 2011: RCP 8.5A scenario of comparatively high greenhouse gas emis-
720 sions. *Climatic Change*, **109** (1-2), 33–57.
- 721 Rowell, D. P., and R. G. Jones, 2006: Causes and uncertainty of future summer drying over europe.
722 *Climate Dynamics*, **27** (2-3), 281–299.
- 723 Salathé Jr, E. P., R. Steed, C. F. Mass, and P. H. Zahn, 2008: A High-Resolution Climate Model
724 for the US Pacific Northwest: Mesoscale Feedbacks and Local Responses to Climate Change*.
725 *Journal of Climate*, **21** (21), 5708–5726.
- 726 Scoccimarro, E., M. Zampieri, A. Bellucci, A. Navarra, and Coauthors, 2013: Heavy precipitation
727 events in a warmer climate: results from CMIP5 models. *Journal of climate*.

- 728 Seneviratne, S. I., and Coauthors, 2012: Changes in climate extremes and their impacts on the
729 natural physical environment. *Managing the risks of extreme events and disasters to advance*
730 *climate change adaptation*, 109–230.
- 731 Sillmann, J., V. Kharin, F. Zwiers, X. Zhang, and D. Bronaugh, 2013: Climate extremes indices
732 in the cmip5 multimodel ensemble: Part 2. future climate projections. *Journal of Geophysical*
733 *Research: Atmospheres*, **118 (6)**, 2473–2493.
- 734 Simmons, A., K. Willett, P. Jones, P. Thorne, and D. Dee, 2010: Low-frequency variations
735 in surface atmospheric humidity, temperature, and precipitation: Inferences from reanalyses
736 and monthly gridded observational data sets. *Journal of Geophysical Research: Atmospheres*,
737 **115 (D1)**.
- 738 Singh, D., M. Tsiang, B. Rajaratnam, and N. S. Diffenbaugh, 2013: Precipitation extremes over the
739 continental United States in a transient, high-resolution, ensemble climate model experiment.
740 *Journal of Geophysical Research: Atmospheres*, **118 (13)**, 7063–7086.
- 741 Small, R. J., and Coauthors, 2014: A new synoptic scale resolving global climate simulation using
742 the community earth system model. *Journal of Advances in Modeling Earth Systems*, **6 (4)**,
743 1065–1094.
- 744 Staniforth, A. N., and H. L. Mitchell, 1978: A variable-resolution finite-element technique for
745 regional forecasting with the primitive equations. *Monthly Weather Review*, **106 (4)**, 439–447.
- 746 Sugi, M., and J. Yoshimura, 2004: A mechanism of tropical precipitation change due to co2
747 increase. *Journal of climate*, **17 (1)**, 238–243.

- 748 Taschetto, A. S., A. S. Gupta, N. C. Jourdain, A. Santoso, C. C. Ummenhofer, and M. H. England,
749 2014: Cold tongue and warm pool enso events in cmip5: mean state and future projections.
750 *Journal of Climate*, **27 (8)**, 2861–2885.
- 751 Taylor, M. A., 2011: Conservation of mass and energy for the moist atmospheric primitive equa-
752 tions on unstructured grids. *Numerical Techniques for Global Atmospheric Models*, Springer,
753 357–380.
- 754 Tebaldi, C., K. Hayhoe, J. M. Arblaster, and G. A. Meehl, 2006: Going to the extremes. *Climatic
755 change*, **79 (3-4)**, 185–211.
- 756 Trenberth, K. E., 2011: Changes in precipitation with climate change. *Climate Research*, **47 (1)**,
757 123.
- 758 Trenberth, K. E., A. Dai, R. M. Rasmussen, and D. B. Parsons, 2003: The changing character of
759 precipitation. *Bulletin of the American Meteorological Society*, **84 (9)**, 1205–1217.
- 760 Walker, M. D., and N. S. Diffenbaugh, 2009: Evaluation of high-resolution simulations of daily-
761 scale temperature and precipitation over the united states. *Climate dynamics*, **33 (7-8)**, 1131–
762 1147.
- 763 Wehner, M. F., 2013: Very extreme seasonal precipitation in the NARCCAP ensemble: model
764 performance and projections. *Climate Dynamics*, **40 (1-2)**, 59–80.
- 765 Wehner, M. F., R. L. Smith, G. Bala, and P. Duffy, 2010: The effect of horizontal resolution
766 on simulation of very extreme US precipitation events in a global atmosphere model. *Climate
767 dynamics*, **34 (2-3)**, 241–247.

- 768 Wehner, M. F., and Coauthors, 2014: The effect of horizontal resolution on simulation qual-
769 ity in the Community Atmospheric Model, CAM5.1. *J. Model. Earth. Sys.*, doi:10.1002/
770 2013MS000276.
- 771 Yoon, J.-H., S. S. Wang, R. R. Gillies, B. Kravitz, L. Hipps, and P. J. Rasch, 2015: Increasing
772 water cycle extremes in California and in relation to ENSO cycle under global warming. *Nature*
773 *communications*, **6**.
- 774 Zarzycki, C. M., C. Jablonowski, and M. A. Taylor, 2014: Using Variable-Resolution Meshes
775 to Model Tropical Cyclones in the Community Atmosphere Model. *Monthly Weather Review*,
776 **142** (3), 1221–1239.
- 777 Zarzycki, C. M., C. Jablonowski, D. R. Thatcher, and M. A. Taylor, 2015: Effects of localized grid
778 refinement on the general circulation and climatology in the Community Atmosphere Model.
779 *Journal of Climate*, **(2015)**.
- 780 Zhang, X., L. Alexander, G. C. Hegerl, P. Jones, A. K. Tank, T. C. Peterson, B. Trewin, and
781 F. W. Zwiers, 2011: Indices for monitoring changes in extremes based on daily temperature and
782 precipitation data. *Wiley Interdisciplinary Reviews: Climate Change*, **2** (6), 851–870.
- 783 Zhang, X., J. Wang, F. W. Zwiers, and P. Y. Groisman, 2010: The influence of large-scale climate
784 variability on winter maximum daily precipitation over North America. *Journal of Climate*,
785 **23** (11), 2902–2915.
- 786 update the mesh grid plot
- 787 update the plot with new label levels

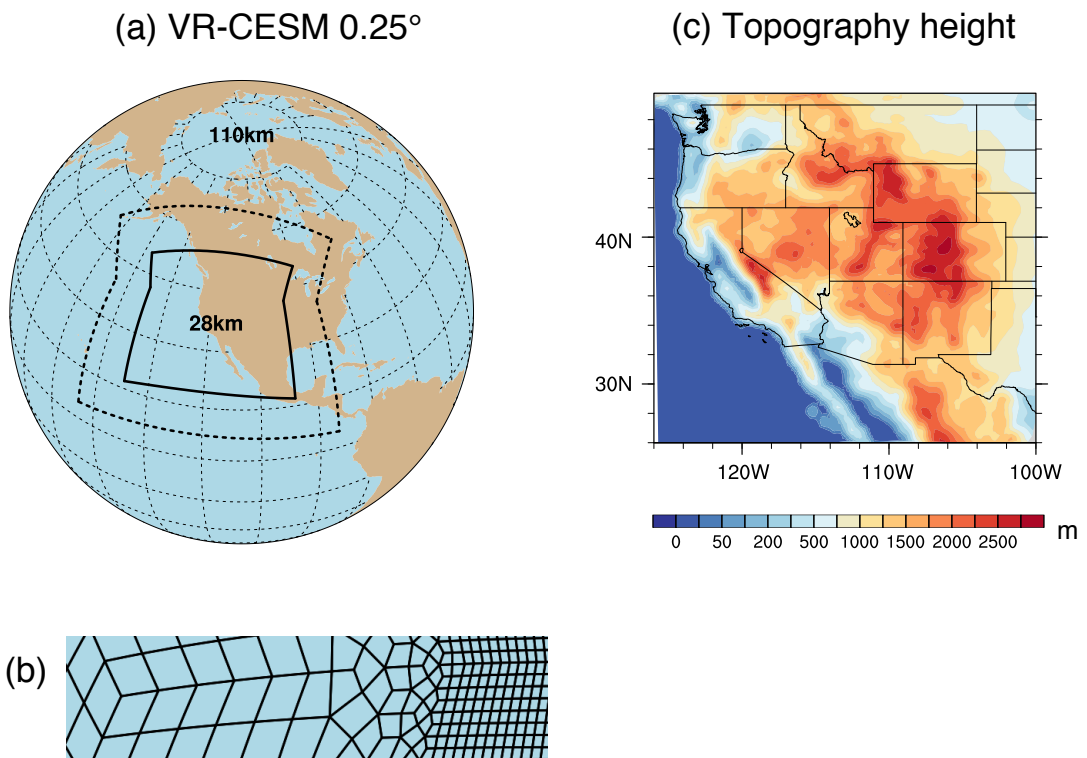
788 LIST OF TABLES

TABLE 1. Precipitation indices employed in this study.

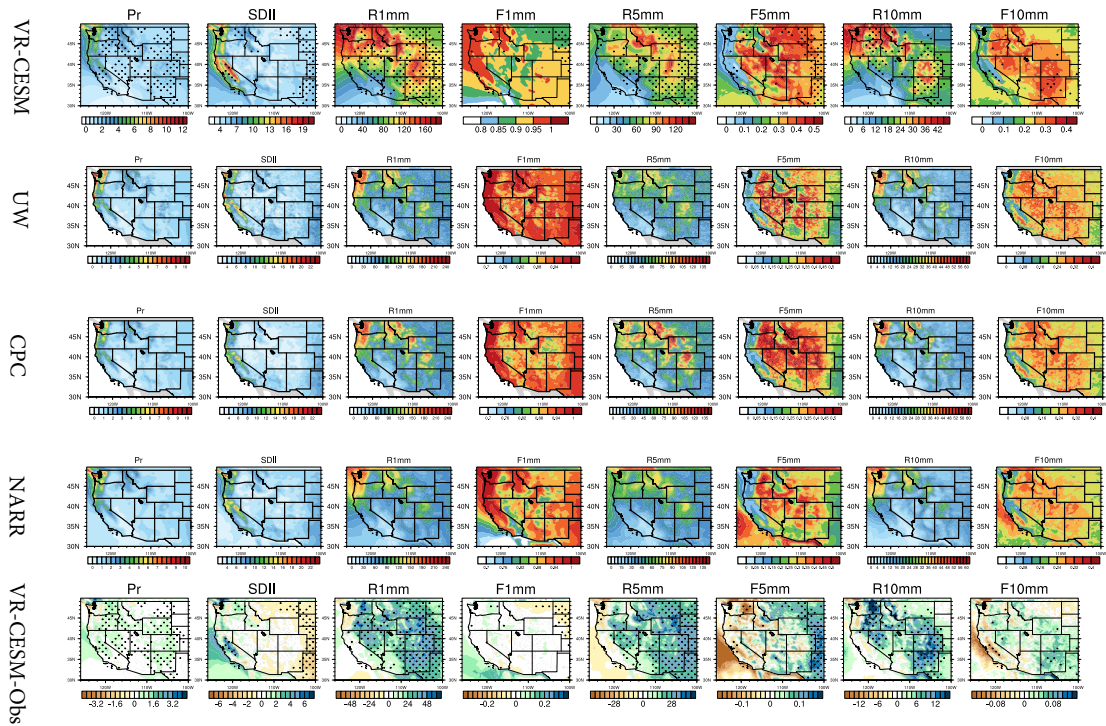
Name	Definition
Pr	Mean daily precipitation
R1mm	Number of days per year with Pr>1 mm
SDII	Simple precipitation intensity index: Precipitation amount / $\langle R1mm \rangle$ (mm/day)
R5mm	Number of days per year with Pr>1 mm and Pr=<5 mm
R10mm	Number of days per year with Pr>5 mm and Pr=<10 mm
R20mm	Number of days per year with Pr>10 mm and Pr=<20 mm
R40mm	Number of days per year with Pr>20 mm and Pr=<40 mm
Rxmm	Number of days per year with Pr>40 mm
F1mm	Fraction of precipitation contributed to the total precipitation for days of R1mm (similarly for F5mm, F10mm, F20mm, F40mm and Fxmm)
P5mm	Precipitation amount from R5mm (similarly for P10mm, P20mm, F40mm, Pxmm)

790 **LIST OF FIGURES**

791 Fig. 1.	(a) The approximate grid spacing used for the VR-CESM 0.25° mesh. (b) A depiction of 792 the transition from the global 1° resolution mesh through two layers of refinement to 0.25° . 793 (c) Topography height over the study area.	41
794 Fig. 2.	Mean precipitation and other related indices from VR-CESM and reference datasets over 795 1980-2005. (Note: Grids with statistically significance difference are marked with stip- 796 pling.)	42
797 Fig. 3.	The mean precipitation and other related indices from VR-CESM and reference datasets 798 over 1980-2005 (continued).	43
799 Fig. 4.	The mean precipitation (Pr), 2m average temperature ($T2avg$), and 2m relative humidity 800 (RH) averaged over each time period. (Note: Grids with statistically significance difference 801 for the RH are marked with stippling.)	44
802 Fig. 5.	Differences of precipitation behaviors from past to future over WUS averaged of each time 803 period. (Note: Grids with statistically significance difference are marked with stippling.)	45
804 Fig. 6.	Differences of precipitation behaviors from past to future over WUS averaged of each time 805 period (continued).	46
806 Fig. 7.	Changes of specific humidity and horizontal wind pattern at 850hPa for moisture flux il- 807 lustration, and IVT for simulations under different time period of wet season (October to 808 March). (Note: The minimum wind vector is set to be 0.5 m/s, therefore, the wind less than 809 0.5 m/s is also plotted at the minimum length for better visualization.) For all difference 810 plots, make sure to use a common [min,max] range as its currently difficult to tease out dif- 811 ferences. Difference plots should also use a different color table to the mean results (perhaps 812 a single color color table?).	47
813 Fig. 8.	Difference of precipitation behaviors between warm and cool phases of ENSO from past to 814 future over WUS averaged of each time period.	48
815 Fig. 9.	Changes of IVT for simulations under different phases of ENSO of wet season (October to 816 March). (Note: The minimum wind vector is set to be 0.5 m/s, therefore, the wind less than 817 0.5 m/s is also plotted at the minimum length for better visualization.)	49

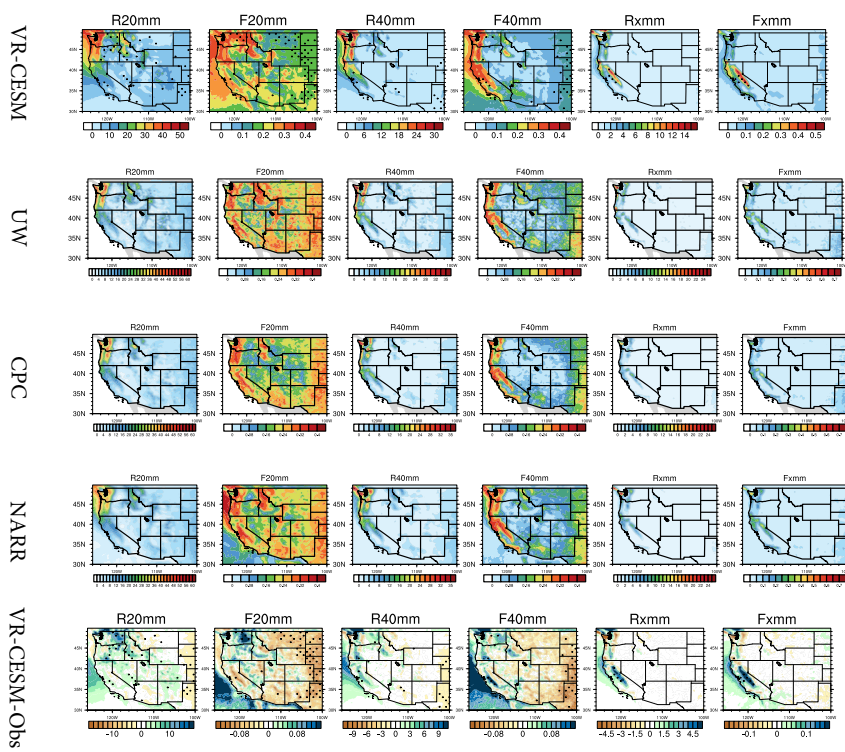


818 FIG. 1. (a) The approximate grid spacing used for the VR-CESM 0.25° mesh. (b) A depiction of the transition
 819 from the global 1° resolution mesh through two layers of refinement to 0.25° . (c) Topography height over the
 820 study area.

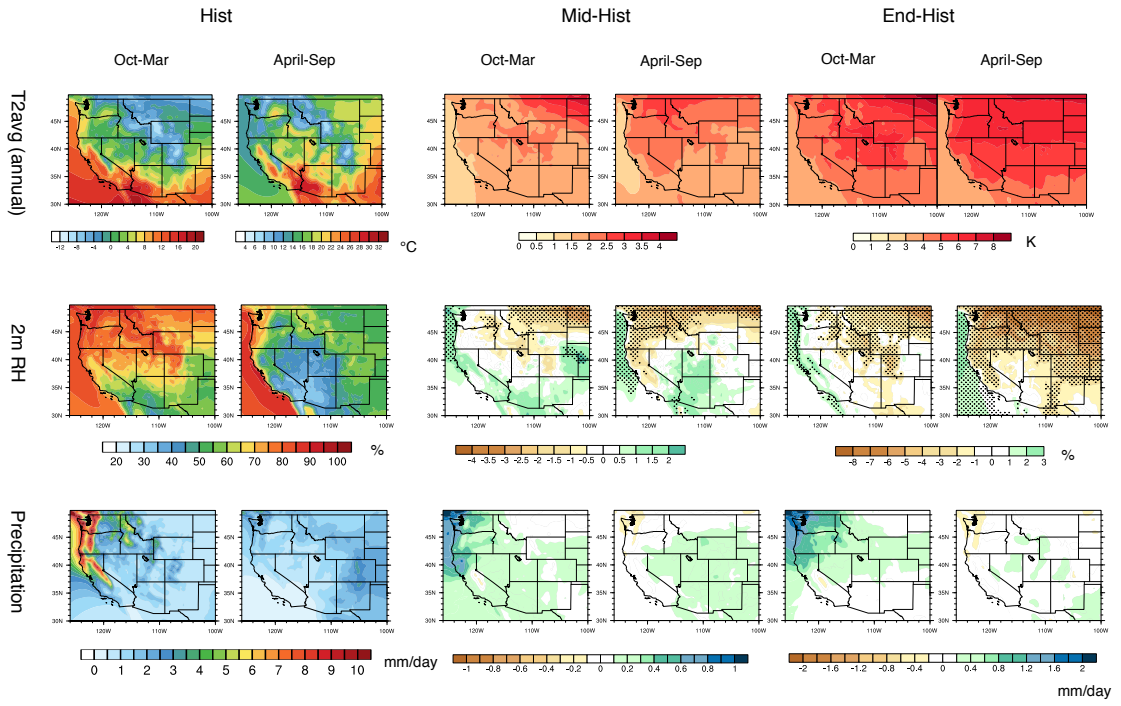


821 FIG. 2. Mean precipitation and other related indices from VR-CESM and reference datasets over 1980-2005.

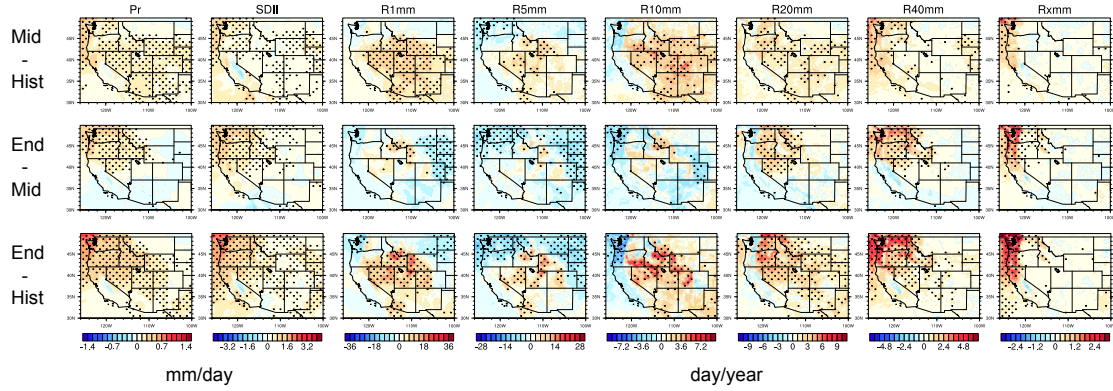
822 (Note: Grids with statistically significant difference are marked with stippling.)



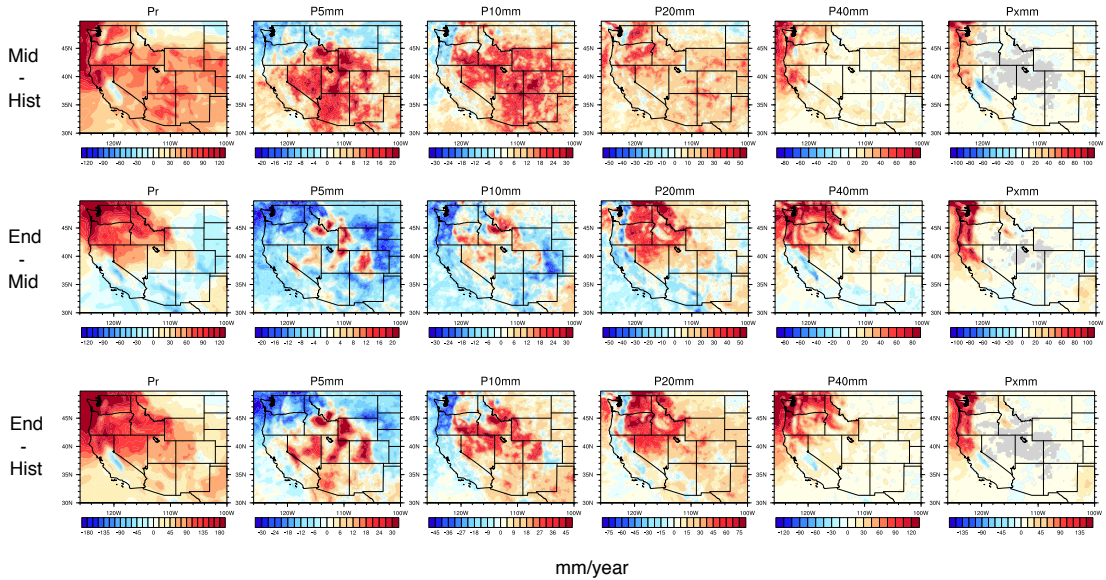
823 FIG. 3. The mean precipitation and other related indices from VR-CESM and reference datasets over 1980-
 824 2005 (continued).



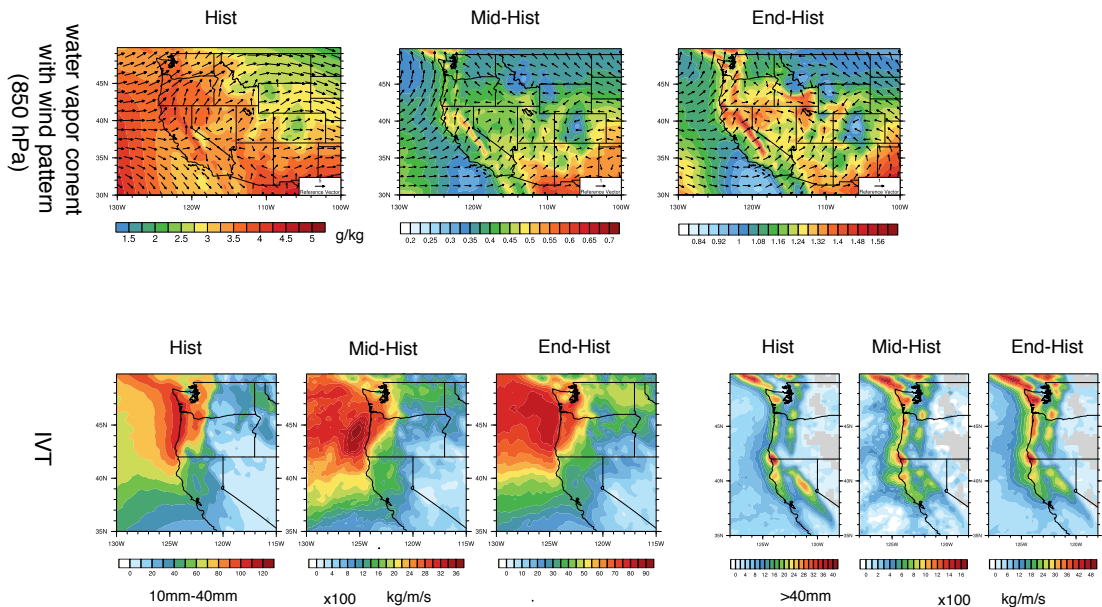
825 FIG. 4. The mean precipitation (Pr), 2m average temperature (T2avg), and 2m relative humidity (RH) aver-
 826 aged over each time period. (Note: Grids with statistically significance difference for the RH are marked with
 827 stippling.)



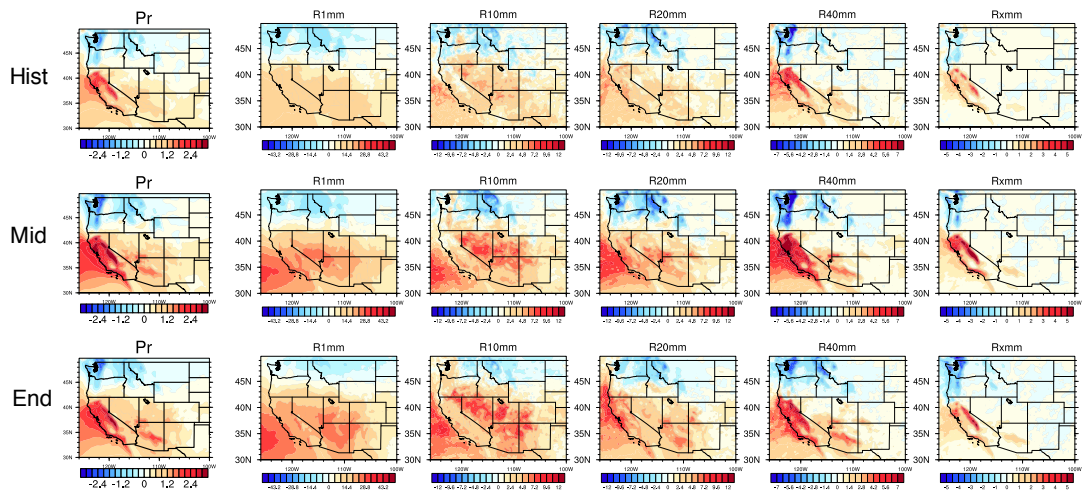
828 FIG. 5. Differences of precipitation behaviors from past to future over WUS averaged of each time period.
 829 (Note: Grids with statistically significance difference are marked with stippling.)



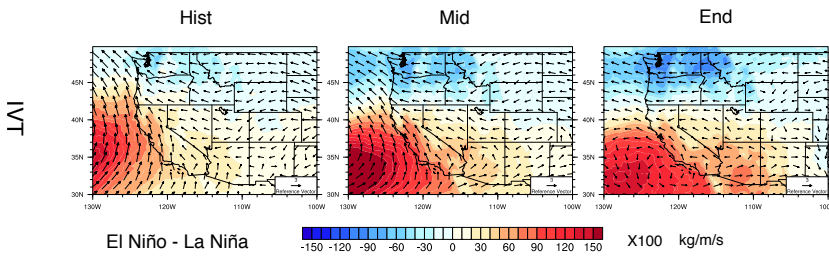
830 FIG. 6. Differences of precipitation behaviors from past to future over WUS averaged of each time period
 831 (continued).



832 FIG. 7. Changes of specific humidity and horizontal wind pattern at 850hPa for moisture flux illustration, and
 833 IVT for simulations under different time period of wet season (October to March). (Note: The minimum wind
 834 vector is set to be 0.5 m/s, therefore, the wind less than 0.5 m/s is also plotted at the minimum length for better
 835 visualization.) For all difference plots, make sure to use a common [min,max] range as its currently difficult
 836 to tease out differences. Difference plots should also use a different color table to the mean results (perhaps a
 837 single color color table?). 47



838 FIG. 8. Difference of precipitation behaviors between warm and cool phases of ENSO from past to future
 839 over WUS averaged of each time period.



840 FIG. 9. Changes of IVT for simulations under different phases of ENSO of wet season (October to March).
 841 (Note: The minimum wind vector is set to be 0.5 m/s, therefore, the wind less than 0.5 m/s is also plotted at the
 842 minimum length for better visualization.)